

- taining yeast cells and retested for two-hybrid readouts. This step eliminates false positives probably resulting from *cis*- and *trans*-acting mutations that can influence reporter gene activity (17).
21. R. Durbin and J. Thierry-Mieg, in *Computational Methods in Genome Research*, S. Suhai, Ed. (Plenum, New York, 1994).
 22. <http://cancerbiology.dfci.harvard.edu/cancerbiology/ResLabs/Vidal/>
 23. www.proteome.com/databases/index.htm
 24. <http://cmgm.stanford.edu/~kimlab/wmdirectorybig.html>
 25. D. S. Sieburth, Q. Sun, M. Han, *Cell* **94**, 119 (1998).
 26. C. Bai et al., *Cell* **86**, 263 (1996).
 27. A. Kikuchi, S. D. Demo, Z. H. Ye, Y. W. Chen, L. T. Williams, *Mol. Cell. Biol.* **14**, 7483 (1994).
 28. F. Solari, A. Bateman, J. Ahninger, *Development* **126**, 2483 (1999).
 29. Y. Xue et al., *Mol. Cell.* **2**, 851 (1998).
 30. R. L. Tatusov, E. V. Koonin, D. J. Lipman, *Science* **278**, 631 (1997).
 31. J. A. Printen and G. F. Sprague, *Genetics* **138**, 609 (1994); K. Y. Choi, B. Satterberg, D. M. Lyons, E. A. Elion, *Cell* **78**, 499 (1994).
 32. For yet unknown reasons, several proteins notoriously behave as promiscuous interactors in the context of the two-hybrid system. Because such promiscuous interactors would bias the clustering analysis, they should systematically be removed from the analysis. In the AD-wrmcDNA library, this is the case for AD-PAL-1, AD-UNC-15, AD-F33G12.5, and AD-F54D5.5, which were found as potential ISTs for several vORF baits but also for unrelated baits such as DB-LIN-5, DB-LIN-6, DB-MEX-3, DB-OSM-10, and DB-PCT-1 (A. J. M. Walhout, M. Lorson, S. van den Heuvel, N. Huang, C. Hunter, A. Sugimoto, A. Hart, M. Vidal, unpublished data).
 33. S. G. Clark, X. Lu, H. R. Horvitz, *Genetics* **137**, 987 (1994); L. S. Huang, P. Tzou, P. W. Sternberg, *Mol. Biol. Cell* **5**, 395 (1994); X. Lu and H. R. Horvitz, in preparation.
 34. R. K. Herman and E. M. Hedgecock, *Nature* **348**, 169 (1990).
 35. In summary, the two-hybrid readouts are excellent for LIN-53(RbAp48)/LIN-37 (interaction was detected multiple times in both DB-X/AD-Y and DB-Y/AD-X orientations, with full-length proteins in the matrix, scores positive for three reporter genes and belongs

to clusters) and the available biological information on both proteins is consistent with an interaction (both proteins are required for a synMuv function and co-localize). Because no interolog has been identified yet for this interaction, it is possible that its study in *C. elegans* might reveal new features of pRB function in humans.

36. A. J. M. Walhout, H. Endoh, M. Vidal, data not shown.
37. We thank N. Dyson, F. Holstege, L. Matthews, and S. van den Heuvel for comments on the manuscript; M. Chalfie, A. Coulson, E. Harlow, H. R. Horvitz, S. Kim, E. Lander, M. Murray, R. Plasterk, J. and D. Thierry-Mieg, and S. van den Heuvel for support; J. Hitti, L. Doucette-Stamm, and B. Guild (Genome Therapeutics Corp., Waltham, MA) for their help with sequencing; H. Endoh, H. R. Horvitz, S. Kim, M. Lorson, and S. van den Heuvel for reagents or unpublished information, or both; and C. Ngwu for generous help with the design of our Web site. Supported by grants 1 RO1 HG01715-01 (National Human Genome Research Institute) and 1 R21 CA81658 A 01 (National Cancer Institute) awarded to M.V.

9 August 1999; accepted 19 November 1999

A Short Fe-Fe Distance in Peroxidiferic Ferritin: Control of Fe Substrate Versus Cofactor Decay?

Jungwon Hwang,¹ Carsten Krebs,² Boi Hanh Huynh,² Dale E. Edmondson,³ Elizabeth C. Theil,⁴ James E. Penner-Hahn^{1*}

The reaction of oxygen with protein diiron sites is important in bioorganic syntheses and biomineralization. An unusually short Fe-Fe distance of 2.53 angstroms was found in the diiron (μ -1,2 peroxidiferic) intermediate that forms in the early steps of ferritin biomineralization. This distance suggests the presence of a unique triply bridged structure. The Fe-Fe distances in the μ -1,2 peroxidiferic complexes that were characterized previously are much longer (3.1 to 4.0 angstroms). The 2.53 angstrom Fe-Fe distance requires a small Fe-O-O angle ($\sim 106^\circ$ to 107°). This geometry should favor decay of the peroxidiferic complex by the release of H_2O_2 and μ -oxo or μ -hydroxo diferric biomineral precursors rather than by oxidation of the organic substrate. Geometrical differences may thus explain how diiron sites can function either as a substrate (in ferritin biomineralization) or as a cofactor (in O_2 activation).

Iron proteins mediate iron and oxygen chemistry for a variety of biological functions. Although heme proteins may be the most familiar, nonheme diiron proteins are widely distributed. Reactions of iron and oxygen at carboxylate-bridged diiron centers include reversible O_2 binding for respiration (hemerythrin), oxidation and desaturation of organic substrates [methane monooxygenase (MMOH), the R2 subunit of

ribonucleotide reductase, and the stearyl-acyl carrier protein Δ -9 desaturase (Δ 9D)], and concentration of iron in a ferric biomineral (ferritin) (1, 2). Ferritins are ubiquitous proteins that concentrate iron in cells as a mineral, storing the iron for later use; cytotoxic reactions of both Fe^{2+} and O_2 are controlled by ferritin chemistry. Ferric oxo reaction products are transported within ferritin to a large cavity in the center of the protein to form a ferric oxide hydrate. The recent detection of a peroxidiferic intermediate in the ferritin ferroxidase reaction (3, 4) firmly establishes the ferritin ferroxidase site as very similar to sites in the O_2 -activating diiron enzymes (Fig. 1). What is puzzling is how the peroxidiferic intermediate can be a catalytic cofactor in the enzymes but a substrate intermediate in the ferritins.

Similarities among the peroxidiferic intermediates of MMOH (5) and site-specific mutants of R2 (6), Δ 9D (7), and ferritin (3, 4) include a distinct blue color from a peroxo \rightarrow Fe charge transfer band (650 to 725 nm), a relatively large Mössbauer isomer shift (0.62 to 0.66 mm/s) that is characteristic of Fe^{3+} -peroxide complexes, and high-frequency (850 to 900 cm^{-1}) Raman bands that are attributable to a μ -1,2 peroxide O-O stretch (Table 1). These spectroscopic similarities stand in contrast to the reactivities of the peroxidiferic intermediates in the different proteins. Decay of the peroxo intermediate yields a high-valence Fe oxidant in the O_2 -activating enzymes but gives diferric oxo-hydroxo biomineral precursors in ferritin (Fig. 1).

To obtain further insight into the ferritin reaction, we used x-ray absorption spectroscopy (XAS), which includes x-ray absorption near edge structure (XANES) and extended x-ray absorption fine structure (EXAFS), to examine the structure of the ferritin peroxidiferic intermediate that is formed when recombinant frog M ferritin reacts with Fe^{2+} and O_2 . We observed a short Fe-Fe separation of 2.53 Å in the intermediate that allows us to define the diiron structure and to gain insight into the features responsible for modulating the peroxidiferic decay pathway.

Two intermediates in the ferritin reaction with Fe^{2+} and O_2 were trapped by rapid freeze quench at 25 ms ($+O_2^{25\text{ ms}}$) or at 1 s ($+O_2^1\text{ s}$) and were packed in delrin sample cells that are suitable for Mössbauer and XAS measurements (3, 4, 8, 9). A third sample, which was prepared in the absence of O_2 , provided an Fe^{2+} control. Mössbauer measurements (Table 2) were made both before and after x-ray irradiation to ensure sample integrity and to quantify the different iron species. In the $-O_2$ samples, most of the iron is high-spin Fe^{2+} , with a linewidth that suggests a mixture of several similar Fe^{2+} structures (denoted 1). After 25-ms reaction

¹Department of Chemistry, University of Michigan, Ann Arbor, MI 48109-1055, USA. ²Department of Physics, ³Departments of Biochemistry and Chemistry, Emory University, Atlanta, GA 30322, USA. ⁴Children's Hospital Oakland Research Institute, 5700 Martin Luther King Jr. Way, Oakland, CA 94609-1673, USA.

*To whom correspondence should be addressed. E-mail: jeph@umich.edu

with O_2 , ~70% of the iron is the peroxodiferrous intermediate species (denoted 2), and the remainder is Fe^{2+} . At 1 s, the peroxodiferrous species has decayed, and >90% of the Fe is μ -oxo or μ -hydroxo diferric products, or both (denoted 3). The XAS spectra were obtained under standard conditions (10). Seven to 12 scans were averaged for each sample, and two or three independent samples were measured for each species (Table 2). Data reduction (11) and analysis (12) followed standard procedures.

The XANES spectra for one set of samples ($+O_2^{25\text{ ms}}$, $+O_2^{1\text{ s}}$, and $-O_2$) are shown in Fig. 2A. The edge for the $-O_2$ sample is consistent with Fe^{2+} (13), whereas that for $+O_2^{1\text{ s}}$ is shifted to higher energy by ~3 eV, which is consistent with formation of Fe^{3+} . There is a slightly smaller edge shift for $+O_2^{25\text{ ms}}$, which reflects incomplete oxidation after 25 ms. The $+O_2^{25\text{ ms}}$ spectrum can be modeled as a 25:75 ratio of the $-O_2$ and $+O_2^{1\text{ s}}$ spectra, which is in excellent agreement with the Mössbauer quantitation (Table 2) and supports the assignment of 2 as a ferric species. The $1s \rightarrow 3d$ transition is extremely weak for all three ferritin samples and shows only a small increase in energy for the oxidized samples. Weak $1s \rightarrow 3d$ transitions are characteristic of nearly centrosymmetric 6-coordinate iron sites (14), which suggests that the average coordination number is 5 to 6 (15).

Fourier transforms of the EXAFS data are shown in Fig. 2B and fitting results are summarized in Table 2. Detailed fits and plots are given in supplemental data (16). The dominant feature of each spectrum is a peak at $R + \alpha \approx 1.55 \text{ \AA}$ (where R is absorber-scatterer distance and α is EXAFS phase shift) that can be modeled as an Fe-O shell at $\approx 2.0 \text{ \AA}$. The best single-shell fits give unrealistically low coordination numbers of 3 to 4, which suggests disorder in the Fe-O distances (17). Two-shell fits (1 to 2 Fe-O at 1.92 \AA and 3 to 4 Fe-O at 2.05 \AA) give more reasonable total coordination numbers but do not give a significant improvement in fit quality (18). The observed Fe-O bond lengths for the Fe^{2+} samples ($-O_2$) are slightly longer than those for the other samples and are consistent with the larger ionic radius of Fe^{2+} . Bond-valence sum calculations (19) using the observed Fe-O distances and assuming ligation by six oxygens give apparent valences of 2.3 and 3.2 for the $-O_2$ and the oxidized samples, respectively, which supports the conclusion that the Fe in each sample is 5- to 6-coordinate.

All samples show additional peaks at higher R , but only for $+O_2^{25\text{ ms}}$ is there a large outer shell peak. This peak, at $R + \alpha \approx 2.25 \text{ \AA}$ (dashed line in Fig. 2B), is well modeled as an Fe-Fe shell at $\approx 2.5 \text{ \AA}$. Attempts to model this feature as C or S gave worse fits and refinements to chemically unreasonable coordination

numbers or Debye-Waller factors, or both. When ΔE_0 (shift in threshold energy) for the Fe-Fe shell was varied, the best fits were found for $\Delta E_0 \approx 0$, as seen previously for metal-metal scattering (8). Determination of the precise Fe-Fe coordination number is complicated by the correlation between coordination number and Debye-Waller factor. However, the best-fit coordination numbers of ≈ 0.5 give chemically reasonable Debye-Waller factors and are consistent with the Mössbauer determination that the $+O_2^{25\text{ ms}}$ samples contain 60 to 75% of 2.

Fig. 1. Comparison of the role of peroxodiferrous-protein complexes during biomineralization (ferritin) and oxygen activation (MMOH). In ferritin (left), the peroxodiferrous complex decays to diferric oxo or hydroxo precursors that are translocated between the catalytic and biomineralization sites and hydrogen peroxide is released (32). In MMOH (right), the decay produces a potent oxidant (Q) that oxidizes organic substrates and forms the diferric product, which is reduced to the initial diferric state by the reduced form of nicotinamide adenine dinucleotide through the reductase, MMR (1).

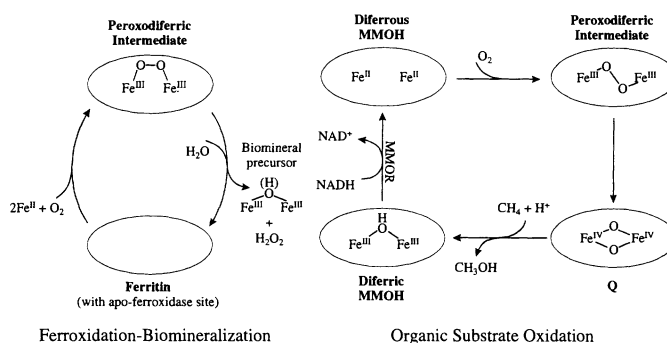
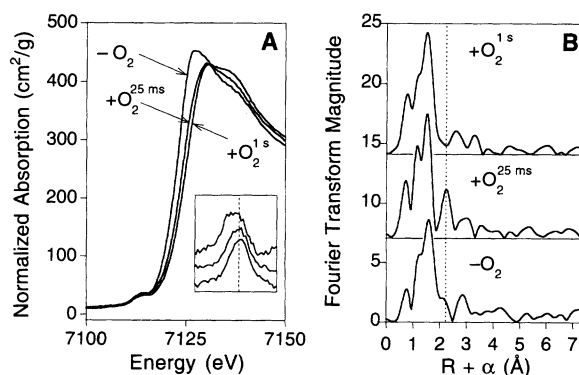


Table 1. Spectroscopic properties of peroxodiferrous intermediates in various proteins and peroxodiferrous compounds. The site-specific R2 mutations are $D^{84} \rightarrow E^{84}$ and $W^{48} \rightarrow F^{48}/D^{84} \rightarrow E^{84}$ (33). The compounds A, C, and D are shown in Fig. 3. ϵ , molar absorbance of band in visible spectra; δ isomer shift in Mössbauer.

Protein or compound	λ_{max} (nm)	ϵ ($M^{-1} \text{ cm}^{-1}$)	δ (mm/s)	ΔE_0 (mm/s)	$\nu_{\text{O-O}}$ (cm^{-1})	Fe-Fe distance (\AA)	Reference no.
M ferritin	650	~1000	0.62	1.06	851	2.53*	(2, 3)
MMOH	725	~1800	0.66	1.51			(4)
R2 mutants	700	~1500	0.63	1.58	870		(5)
$\Delta 9D$	700	~1200	0.68	1.90	898		(6)
			0.64	1.06			
A	694	2650	0.66	1.40	888	4.01	(23)
C	500–800	1700	0.65	1.70		3.33	(25)
			0.58	0.70			
D	494	1100	0.54	1.68	848	3.14	(22)
	648	1200					
	846	230					

*As measured here.

Fig. 2. XAS spectra for precursor, intermediate, and products in the initial oxidation of ferritin biomineralization. (A) XANES spectra with $1s \rightarrow 3d$ transitions (inset). Dashed line at 7113.5 eV shows shift in $1s \rightarrow 3d$ energy. (B) Fourier transforms of the EXAFS data for these samples. Dashed line marks the center of the 2.5 \AA Fe-Fe distance that is specific to the $+O_2^{25\text{ ms}}$ sample.



outer shell peaks for the $-O_2$ samples are not as well modeled by Fe-Fe; these most likely arise from Fe-C interactions, possibly from a histidine ligand.

The 2.53 Å Fe-Fe distance in **2** is unprecedented for μ -carboxylato diferric compounds. Such short Fe-Fe distances have only been reported for the high-valence Fe^{3+}/Fe^{4+} intermediate X in R2 (**8**) and the Fe^{4+}/Fe^{4+} intermediate Q in MMOH (**21**). The structurally characterized μ -1,2 peroxodiferric compounds **A** through **D** are shown schematically in Fig. 3. Their Fe-Fe distances range from 3.1 to 4.0 Å (22–25), with the distance decreasing as the number of bridging ligands increases and as the size of the bridging ligand decreases (carboxylato > alkoxo, hydroxo > oxo). However, none have Fe-Fe distances as short as that found in **2**. Based on these structures and on the correlation between bridging ligands and Mn-Mn distance in dinuclear Mn complexes (**26**), it is likely that two single-atom bridges (for example, μ -1,1-carboxylato, μ -alkoxo, μ -hydroxo, or μ -oxo) are required in addition to the peroxo bridge to

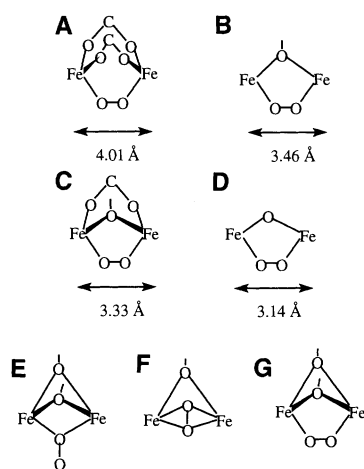


Fig. 3. Various μ -1,2 peroxo diferric centers. Small molecule analogs: **A** (**23**), **B** (**24**), **C** (**25**), and **D** (**22**). Possible structures consistent with the 2.53 Å Fe-Fe distance in the ferritin intermediate: **E** through **G**.

account for the short Fe-Fe distance in **2**. Possible structures for **2** can thus be represented schematically as **E** through **G** (Fig. 3). Structure **E** is inconsistent with the Raman data (**4**) and structure **F** is strongly disfavored by the large value (851 cm^{-1}) for ν_{O-O} (Table 1). In Cu peroxo complexes, the side-on bridging geometry in **F** gives ν_{O-O} values of 750 to 760 cm^{-1} (**27, 28**), nearly 100 cm^{-1} less than values for **2** (**4**). Thus, **G** is the only reasonable structure consistent with all of the available data. Although no small molecule analogs of **G** are known in Fe chemistry to date, precedent for **G** is found in Mn chemistry, where a di- μ -oxo, μ -1,2-peroxo Mn^{4+}/Mn^{4+} dimer has a Mn-Mn distance of 2.53 Å (**29**). With structure **G** and reasonable values for the peroxide bond lengths (Fe-O = 1.90 to 2.00 Å; O-O = 1.40 to 1.45 Å), the Fe-O-O angle, γ , must be quite small, $\approx 106^\circ$ to 107° (**30**). In contrast, structures **A** to **D** have $\gamma = 120^\circ$ to 129° .

The combined spectroscopic data (Table 1) show that **2**, although similar to the other peroxodiferric intermediates, has a distinctive structure. Intermediate **2** has smaller ΔE_Q , maximum wavelength λ_{max} , and ν_{O-O} values than the other proteins and, based on the Fe-Fe distance, has the smallest γ of the structurally characterized peroxodiferric complexes. From a normal-coordinate analysis, Brunold *et al.* (**31**) showed that the Fe-O and O-O stretching frequencies of μ -1,2 peroxodiferric dimers are mechanically coupled and are strongly dependent on γ ; larger γ values give stronger coupling, thus increasing ν_{O-O} and decreasing ν_{Fe-O} . With γ of $\sim 107^\circ$, there will be negligible mechanical coupling of ν_{O-O} and ν_{Fe-O} in **2** (**31**), thus accounting for the low ν_{O-O} . A second consequence of the small γ is that π^*_{σ} bonding will be stronger in **2** (**31**), thus giving greater $\pi^* \rightarrow Fe$ charge transfer and a correspondingly stronger O-O bond than in other peroxodiferric complexes. A stronger O-O bond in ferritin should favor the observed release of hydrogen peroxide (**32**) and the formation of the μ -oxo or μ -hydroxo diferric biomineral

precursors over O-O bond cleavage and formation of high-valence intermediates, as seen for the other peroxodiferric species (Fig. 1).

The distinction between diiron cofactor sites (O_2 -activating enzymes) and diiron substrate sites (ferritins) likely depends on the structures of the peroxodiferric intermediates, and thus on the identity and the geometric arrangement of the amino acids bound to the Fe. In the enzymes, each Fe is ligated to E and H in the conserved, duplicated motif EXXH (**33**). In frog M ferritin, one Fe is ligated to an EXXH motif, and the other is ligated to QXXD (**34**). Codon comparison of E or Q and H or D reveals that four out of six nucleotides (GAG or CAG and CAT or GAT) may be shared, emphasizing that a small difference at the nucleotide level may be sufficient to encode cofactor versus substrate reactivity. In all known animal and plant ferritins, Q (in the QXXD motif of frog M ferritin) is conserved but D can be substituted with A, S, or Q (**34, 35**). This variability in Fe ligation may be important in determining peroxodiferric kinetics and biological specificity. Thus, frog M (QXXD) and frog H (QXXS) ferritins differ in rates of peroxodiferric formation and decay and in cell specificity (**35**), which is consistent with a biological role for these ligands in controlling ferritin activity. How these variations affect the bridging geometry and what role geometry plays in fine-tuning the reactivity of the peroxodiferric intermediates are questions that remain to be answered.

References and Notes

- B. J. Waller and J. D. Lipscomb, *Chem. Rev.* **96**, 2625 (1996); A. L. Feig and S. J. Lippard, *Chem. Rev.* **94**, 759 (1994); G. S. Waldo and E. C. Theil, in *Bioinorganic Systems*, vol. 5 of *Comprehensive Supramolecular Chemistry*, K. S. Suslick, Ed. (Pergamon, Oxford, 1996), pp. 65–89.
- Animals produce H-, L-, and M-type ferritin subunits; the H and M types have a functional diiron site. The subunits coassemble to form cell-specific mixtures. Although the functional significance of the subunit ratio is not fully understood, this ratio is controlled precisely and is fixed at the time of cell differentiation. Plants and bacteria appear to have only a single ferritin subunit of the H type, which contains a functional diiron site.
- A. S. Pereira *et al.*, *Biochemistry* **37**, 9871 (1998).
- P. Moëgne-Loccoz *et al.*, *Biochemistry* **38**, 5290 (1999).
- K. E. Liu *et al.*, *J. Am. Chem. Soc.* **117**, 10174 (1995); A. M. Valentine, S. S. Stahl, S. J. Lippard, *J. Am. Chem. Soc.* **121**, 3876 (1999).
- J. M. Bollinger Jr. *et al.*, *J. Am. Chem. Soc.* **120**, 1094 (1998); P. Moëgne-Loccoz, J. Baldwin, B. A. Ley, T. M. Loehr, J. M. Bollinger Jr., *Biochemistry* **37**, 14659 (1998).
- J. A. Broadwater, J. Ai, T. M. Loehr, J. Sanders-Loehr, B. G. Fox, *Biochemistry* **37**, 14664 (1998); J. A. Broadwater, C. Achim, E. Münck, B. G. Fox, *Biochemistry* **38**, 12197 (1999).
- P. J. Riggs-Gelasco *et al.*, *J. Am. Chem. Soc.* **120**, 849 (1998); P. J. Riggs-Gelasco, thesis, University of Michigan (1994).
- An O_2 -saturated apoferritin solution in 0.2 M Mops buffer (pH 7.0) and 0.2 M NaCl was mixed at 23°C with an equal volume of O_2 -saturated ^{57}Fe -enriched (95% enrichment) FeSO_4 in 0.2 M NaCl and 3.5 mM H_2SO_4 . The final protein concentration after mixing was about $49\ \mu\text{M}$ of 24-polymer ferritin molecule.

Table 2. XAS and Mössbauer analysis of Fe intermediates in ferritin. Best-fit parameters give coordination number of 3 for O, 0.5 for Fe (0.3 for $+O_2^{25\text{ ms}}$, 2). Detailed fits are shown in supplemental data (**16**). Values in parentheses are uncertainties in the least significant digit; estimated uncertainties in R and σ^2 are 0.02 Å and $1 \times 10^{-3}\ \text{Å}^2$, respectively. Quantitation of ferrous (**1**), peroxodiferric (**2**), and ferric oxo/hydroxo species (**3**) determined by Mössbauer measurements. Dashes indicate species not observed.

Sample type; no.	Scatterer O		Scatterer Fe		Composition (%)			Edge energy (eV)	1s \rightarrow 3d area (eV $\times 10^2$)
	R (Å)	σ^2 ($\text{Å}^2 \times 10^3$)	R (Å)	σ^2 ($\text{Å}^2 \times 10^3$)	1	2	3		
$-O_2$; 1	2.06	5.8	3.44	5.2	72 (4)	28 (2)	—	7122.3	12.5
$-O_2$; 2	2.06	6.6	3.43	4.8	85 (4)	15 (2)	—	7122.0	13.6
$+O_2^{25\text{ ms}}$; 1	2.01	8.5	2.50	3.5	35 (3)	64 (3)	—	7124.0	13.6
$+O_2^{25\text{ ms}}$; 2	2.00	8.0	2.53	3.2	25 (3)	75 (3)	—	7124.0	13.3
$+O_2^{25\text{ ms}}$; 3	2.00	6.0	2.53	3.4	27 (3)	73 (3)	—	7123.7	12.9
$+O_2^{1\text{ s}}$; 1	2.00	5.9	2.99	8.1	~5	—	95	7124.8	13.0
$+O_2^{1\text{ s}}$; 2	2.00	5.7	3.00	6.2	9 (3)	—	90	7124.5	14.0

- The Fe:ferritin molecule ratio was kept at 36:1. The reaction of apoferritin with Fe²⁺ and O₂ was quenched at 25 ms when the peroxodiferric intermediate had accumulated maximally, and at 1 s when the intermediate had decayed.
10. The experiment was conducted at 3.0 GeV and 50 to 100 mA, with the use of a Si(220) double-crystal monochromator that was detuned 50%, with an Fe foil internal calibration (first inflection point at 7111.2 eV). We used a 13-element Ge solid-state fluorescence detector (incident count rate <60 kHz per channel, about 3-kHz Fe K α fluorescence counts) at 10 K. The step size was 10 eV in the pre-edge region (6880 to 7080 eV), 0.35 eV in the edge region (7080 to 7140 eV), and 0.05 Å⁻¹ in the EXAFS region (2 to 13 Å⁻¹). Integration times ranged from 1 s in the pre-edge region to 20 s at $k = 13 \text{ \AA}^{-1}$, where k is the photoelectron wavevector.
 11. XANES data were normalized to tabulated x-ray cross sections, EXAFS data were extracted by subtracting a first-order pre-edge polynomial, and then a three-region cubic spline was fitted to the EXAFS. Data converted to k space with $E_0 = 7130 \text{ eV}$ and weighted by k^3 . k space data (1.5 to 11.9, 12.4, and 12.7 Å⁻¹ for -O₂, +O₂^{25 ms}, and +O₂^{1 s} samples, respectively) were Fourier transformed to give the R space data in Fig. 2.
 12. Bond lengths, coordination numbers, and Debye-Waller factors determined from fitting Fourier-filtered data ($R = 1.0$ to 3.2, 1.0 to 3.3, and 1.0 to 3.6 Å for the -O₂, +O₂^{25 ms}, and +O₂^{1 s} samples, respectively) with the use of theoretical amplitude and phase functions calculated with FEFF v.6.01. [J. J. Rehr, J. Mustre de Leon, S. I. Zabinsky, R. C. Albers, *J. Am. Chem. Soc.* **113**, 5135 (1991)], with the scale factor (0.9) and ΔE_0 (10 eV) calibrated from fits to data for crystallographically characterized models. Coordination numbers were fixed at reasonable values, and only R and σ were treated as freely variable parameters. Identical metric parameters were obtained for fits to filtered and unfiltered data. A weighted goodness of fit $F' = F^2/\nu = F^2/(N_{\text{idp}} - N_{\text{var}})$ was used to evaluate the quality of the fit [P. J. Riggs-Gelasco, T. L. Stemmler, J. E. Penner-Hahn, *Coord. Chem. Rev.* **144**, 245 (1995)], where F is the root mean square difference between the fit and the data, N_{idp} is the number of independent data points, and N_{var} is the number of variable parameters.
 13. S. M. Kauzlarich *et al.*, *Inorg. Chem.* **25**, 2781 (1986); J. G. DeWitt *et al.*, *J. Am. Chem. Soc.* **113**, 9219 (1991).
 14. A. L. Roe *et al.*, *J. Am. Chem. Soc.* **106**, 1676 (1984).
 15. T. E. Westre *et al.*, *J. Am. Chem. Soc.* **119**, 6297 (1997).
 16. Supplemental data are available at Science Online at www.sciencemag.org/feature/data/1044838.shl.
 17. M. T. Caudle, P. Riggs-Gelasco, A. K. Gelasco, J. E. Penner-Hahn, V. L. Pecoraro, *Inorg. Chem.* **35**, 3577 (1996).
 18. The refined Fe-O distances differ only by the estimated resolution of the data ($\pi/2k_{\text{max}} \approx 0.13 \text{ \AA}$), which further indicates that these fits are not chemically meaningful.
 19. W. Liu and H. H. Thorp, *Inorg. Chem.* **32**, 4102 (1993).
 20. The Debye-Waller factor was constrained to be the same as those found for the 25-ms sample to permit quantitative comparison of the coordination numbers.
 21. L. Shu *et al.*, *Science* **275**, 515 (1997).
 22. Y. Dong, Y. Zang, L. Shu, E. C. Wilkinson, L. Que Jr., *J. Am. Chem. Soc.* **119**, 12683 (1997).
 23. K. Kim and S. J. Lippard, *J. Am. Chem. Soc.* **118**, 4914 (1996).
 24. Y. Dong, S. Yan, V. G. Young Jr., L. Que Jr., *Angew. Chem. Int. Ed. Engl.* **35**, 618 (1996).
 25. T. Ookubo *et al.*, *J. Am. Chem. Soc.* **118**, 701 (1996).
 26. E. Larson, M. S. Lah, X. Li, J. A. Bonadies, V. L. Pecoraro, *Inorg. Chem.* **31**, 373 (1992).
 27. J. Ling *et al.*, *J. Am. Chem. Soc.* **116**, 7682 (1994).
 28. M. J. Baldwin *et al.*, *J. Am. Chem. Soc.* **114**, 10421 (1992).
 29. U. Bossek, T. Weyhermüller, K. Wieghardt, B. Nuber, J. Weiss, *J. Am. Chem. Soc.* **112**, 6387 (1990).
 30. This assumes that the Fe-O-O-Fe torsion angle is zero. γ would be even smaller for nonzero torsion angles.
 31. T. C. Brunold, N. Tamura, N. Kitajima, Y. Moro-oka, E. I. Solomon, *J. Am. Chem. Soc.* **120**, 5674 (1998).
 32. G. S. Waldo and E. C. Theil, *Biochemistry* **32**, 13261 (1993); X. Yang, Y. Chen-Barrett, P. Arosio, N. D. Chasteen, *Biochemistry* **37**, 9743 (1998).
 33. Single-letter abbreviations for the amino acid residues are as follows: A, Ala; D, Asp; E, Glu; F, Phe; H, His; Q, Gln; S, Ser; and W, Trp.
 34. Y. Ha, D. Shi, G. W. Small, E. C. Theil, N. M. Allewell, *J. Biol. Inorg. Chem.* **4**, 243 (1999); P. Hempstead *et al.*, *J. Mol. Biol.* **268**, 424 (1997).
 35. L. F. Dickey *et al.*, *J. Biol. Chem.* **262**, 7901 (1987); A. Treffry, Z. Zhao, M. A. Quail, J. R. Guest, P. M. Harrison, *Biochemistry* **34**, 15204 (1995); J. Fetter, J. Cohen, D. Danger, J. Sanders-Loehr, E. C. Theil, *J. Biol. Inorg. Chem.* **2**, 652 (1997). Kinetics of diferric peroxo formation and decay in a QXXA ferritin (human H) differ from either the QXXD (frog M) or QXXS (frog H); no information is available for the QXXQ ferritin (maize). In the *Escherichia coli* ferritins, EXXH occurs instead of QXXD, QXXA, or QXXS as the ligands to the second Fe, and the Fe is retained at the diiron site [A. Treffry, Z. Zhao, M. A. Quail, J. R. Guest, P. M. Harrison, *FEBS Lett.* **432**, 213 (1998)].
 36. We thank K. Herlihy, G. W. Small, and A. R. Tipton for assistance in the preparation of the ferritin samples and B. G. Fox for communicating results before publication. Supported in part by grants from NIH (GM-45205 to J.E.P.-H., GM-47295 and GM-58778 to B.H.H. and D.E.E., DK-20251 to E.C.T.). X-ray absorption data were measured at Stanford Synchrotron Radiation Laboratory, which is operated by the U.S. Department of Energy (DOE), Office of Basic Energy Sciences, with additional support from NIH, National Center for Research Resources, and the DOE Office of Biological and Environmental Research.

24 August 1999; accepted 16 November 1999

Modulation of Brain Reward Circuitry by Leptin

Stephanie Fulton, Barbara Woodside, Peter Shizgal*

Leptin, a hormone secreted by fat cells, suppresses food intake and promotes weight loss. To assess the action of this hormone on brain reward circuitry, changes in the rewarding effect of lateral hypothalamic stimulation were measured after leptin administration. At five stimulation sites near the fornix, the effectiveness of the rewarding electrical stimulation was enhanced by chronic food restriction and attenuated by intracerebroventricular infusion of leptin. In contrast, the rewarding effect of stimulating neighboring sites was insensitive to chronic food restriction and was enhanced by leptin in three of four cases. These opposing effects of leptin may mirror complementary changes in the rewarding effects of feeding and of competing behaviors.

Research on the regulation of feeding and energy balance has been galvanized by the sequencing of the *obese (ob)* gene and the expression of its protein product, leptin, a circulating hormone secreted by adipocytes (1). Circulating leptin levels reflect the size of the fat mass (2), and thus, this hormone has been considered as a signal that regulates long-term energy balance. Rodents with homozygous mutations in the *ob* gene (the *ob/ob* mouse) or in the gene for the leptin receptor (the *db/db* mouse or the *fa/fa* rat) manifest profound hyperphagia and obesity. Central or peripheral administration of leptin reverses the obesity syndrome found in *ob/ob* mice, stimulates metabolism, and reduces food intake in lean mice or rats (3).

Among the many ways in which leptin could alter food intake is by reducing the appetitive value of food. Such changes could ensue if leptin were to alter the state of brain reward circuitry. Self-administration of rewarding electrical brain stimulation ("self-stimulation") has long been used to assess the state of

this circuitry. Rats and a wide range of other vertebrates will actively seek out electrical stimulation of certain brain regions, including the lateral hypothalamus (LH) (4). The effect that induces the subject to reinitiate the stimulation is called "brain stimulation reward" (BSR). Weight loss resulting from chronic food restriction has been shown to enhance the rewarding effect of stimulating LH sites close to the fornix (5); this perifornical region has been implicated in the control of feeding and energy balance (6). Thus, one might expect that the rewarding effect produced by stimulation of this region would be influenced by leptin. We tested this hypothesis by measuring leptin-induced changes in self-stimulation of the perifornical hypothalamus.

In the demonstrations by Carr and his co-workers that perifornical self-stimulation is modulated by chronic food restriction (7), the rate at which the rats harvested the electrical rewards was measured as a function of the stimulation frequency. Chronic food restriction shifted the resulting rate-frequency function leftward, toward weaker stimulation strengths; the lower the body weight, the weaker the stimulation required to entice the rats to earn a given number of rewards. We adopted an analogous approach to determine

Center for Studies in Behavioural Neurobiology, Concordia University, Montréal, QC, H3G 1M8, Canada.

*To whom correspondence should be addressed. E-mail: shizgal@CSBN.concordia.ca